J Neurophysiol 101: 1494–1506, 2009.
First published January 21, 2009; doi:10.1152/jn.91149.2008.

Distinct Subtypes of Cholecystokinin (CCK)-Containing Interneurons of the Basolateral Amygdala Identified Using a CCK Promoter-Specific Lentivirus

Aaron M. Jasnow,[1] Kerry J. Ressler,[1,2] Sayamwong E. Hammack,[1] Jasmeer P. Chhatwal,[1] and Donald G. Rainnie[1]

[1]*Department of Psychiatry and Behavioral Sciences, Center for Behavioral Neuroscience, Yerkes Research Center, Emory University School of Medicine, Atlanta, Georgia; and* [2]*Howard Hughes Medical Institute, Chevy Chase, Maryland*

Submitted 17 October 2008; accepted in final form 7 January 2009

Jasnow AM, Ressler KJ, Hammack SE, Chhatwal JP, Rainnie DG. Distinct subtypes of cholecystokinin-containing interneurons of the basolateral amygdala identified using a CCK promoter-specific lentivirus. *J Neurophysiol* 101: 1494–1506, 2009. First published January 21, 2009; doi:10.1152/jn.91149.2008. The basolateral amygdala (BLA) is critical for the formation of emotional memories. Little is known about the physiological properties of BLA interneurons, which can be divided into four subtypes based on their immunocytochemical profiles. Cholecystokinin (CCK) interneurons play critical roles in feedforward inhibition and behavioral fear responses. Evidence suggests that interneurons within a subgroup can display heterogeneous physiological properties. However, little is known about the physiological properties of CCK interneurons in the BLA and/or whether they represent a homogeneous or heterogeneous population. To address this question, we generated a lentivirus-expressing GFP under the control of the CCK promoter to identify CCK neurons in vivo. We combined this with whole cell patch-clamp recording techniques to examine the physiological properties of CCK-containing interneurons of the rat BLA. Here, we describe the physiological properties of 57 cells recorded in current-clamp mode; we used hierarchical cluster and discriminant function analysis to demonstrate that CCK interneurons can be segregated into three distinct subtypes (I, II, III) based on their passive and active membrane properties. Additionally, Type II neurons could be further separated into adapting and nonadapting types based on their rates of spike frequency adaptation. These data suggest that CCK interneurons of the BLA are a heterogeneous population and may be functionally distinct subpopulations that differentially contribute to the processing of emotionally salient stimuli.

INTRODUCTION

The basolateral amygdala (BLA) is critical for the generation of emotional behavior and the formation of emotional memories (Davis 1997; Davis and Aggleton 2000; Maren and Fanselow 1996). Extensive studies have shown that the lateral and basolateral amygdala play an important role in the acquisition and expression of conditioned fear (Apergis-Schoute et al. 2005; Campeau and Davis 1995; Campeau et al. 1992; Clugnet and LeDoux 1990; Josselyn et al. 2001; Liang et al. 1994; Muller et al. 1997; Sananes and Davis 1992). Moreover, recent functional imaging studies in humans suggest that increased activity of the amygdala plays a critical role in the etiology of several psychiatric disorders (Protopopescu et al. 2005; Rauch et al. 2000). However, understanding the neural mechanisms underlying emotional information processing ultimately requires knowledge of the anatomy and physiology of its constituent neurons.

The BLA is composed of an intrinsic circuitry that consists of two main neuronal cell types: excitatory glutamatergic pyramidal-like projection neurons and inhibitory GABAergic interneurons (McDonald 1992, 1996; McDonald and Pearson 1989). Subpopulations of GABAergic BLA interneurons contain calcium-binding proteins (parvalbumin [PV], calbindin [CB], and calretinin [CR]) as well as neuropeptides, including vasoactive intestinal peptide (VIP), neuropeptide Y (NPY), somatostatin (SST), and cholecystokinin (CCK) (Mascagni and McDonald 2003; McDonald 1989; McDonald and Betette 2001; McDonald and Mascagni 2001a, 2002; McDonald and Pearson 1989; Muller et al. 2005). Evidence suggests that these BLA interneurons can be divided into four distinct subpopulations identified by their immunocytochemical staining: *1*) PV^+ neurons, a majority of which are CB^+; *2*) SST^+ neurons, a majority of which are also CB^+; *3*) large, multipolar CCK^+ neurons that may also express CB; and *4*) small bipolar and bitufted interneurons that may coexpress to varying degrees, VIP, CR, and CCK (Mascagni and McDonald 2003; McDonald and Betette 2001; McDonald and Mascagni 2001a, 2002). These interneuronal subpopulations are remarkably similar to the interneuron populations described in the cerebral cortex and hippocampus (Kawaguchi and Kubota 1998).

Interneurons of the BLA play an important role in regulating the activity of pyramidal neurons within this region and, because of their differential innervation of BLA pyramidal neurons (Muller et al. 2003, 2007; Smith et al. 2000), each interneuron subtype is thought to provide a unique function to the intrinsic circuitry of the BLA. The synaptology of BLA interneurons has been well documented through immunohistochemical studies. However, only a few studies have examined the physiological properties of BLA interneurons (Kaneko et al. 2008; Rainnie 1999; Rainnie et al. 2006; Szinyei et al. 2000, 2003, 2007; Woodruff and Sah 2007a,b) and little is known about the physiological properties of most of the four interneuron subtypes within the BLA. Moreover, it is not clear whether the interneurons within each subtype are homogeneous or represent a functionally heterogeneous population of cells.

CCK^+ neurons are a critical component of the inhibitory circuitry within the BLA; their pattern of innervation of local

Address for reprint requests and other correspondence: A. M. Jasnow, Center for Behavioral Neuroscience, Emory University, Yerkes Neuroscience Building Rm 5224, 954 Gatewood Road NE, Atlanta, GA 30329 (E-mail: ajasnow@emory.edu).

The costs of publication of this article were defrayed in part by the payment of page charges. The article must therefore be hereby marked "*advertisement*" in accordance with 18 U.S.C. Section 1734 solely to indicate this fact.

pyramidal neurons suggests that they can strongly modulate pyramidal cell excitability as well as synaptic integration (Katona et al. 2001; Mascagni and McDonald 2003). Within the BLA CCK^+ neurons have been classified into two types based mainly on soma size and dendrite thickness. Type L (large) CCK^+ neurons colocalize calbindin, whereas type S (small) CCK^+ neurons colocalize with VIP and/or calretinin (Mascagni and McDonald 2003). CCK is a potent anxiogenic in rodents and may contribute to panic disorder in humans (Belcheva et al. 1994; Chen et al. 2006; Kennedy et al. 1999). Consistent with this hypothesis, activation of CCK receptors in the BLA impairs the extinction of fear memories and CCK antagonists reverse the blockade of extinction induced with cannabinoid receptor type 1 (CB1) receptor antagonists (Chhatwal et al. 2009). In addition, a small population of type L CCK^+ cells of the BLA express the 5-HT_3 serotonin receptor subtype (5-HT3R) (Mascagni and McDonald 2007; Morales and Bloom 1997), suggesting that 5-HT may exert its anxiolytic effects on fear and anxiety via modulation of γ-aminobutyric acid (GABA) and CCK neurotransmission. In the cerebral cortex, two types of CCK^+ cells have been identified physiologically: *1*) regular-spiking and *2*) burst-spiking neurons (Kawaguchi and Kubota 1998). However, no studies to date have characterized the physiological properties of CCK^+ interneurons of the BLA. Here, we used a lentiviral vector expressing GFP under the control of the CCK promoter to identify CCK^+ interneurons within the BLA of rats and record their physiological properties. We used unsupervised cluster analysis and discriminant function analysis (DFA) in a hypothesis-neutral approach to determine whether CCK^+ neurons of the BLA are a single homogeneous group or represent several physiologically distinct groups. We demonstrate that CCK^+ interneurons of the BLA constitute three physiologically distinct subtypes, suggesting that there is considerable electrophysiological, and perhaps functional, heterogeneity within this interneuron population.

METHODS

Animals and housing conditions

All experiments were conducted on male Sprague–Dawley rats at 40–48 days of age (~14 days after virus infusion). All rats were group-housed four per cage in Plexiglas cages with corn cob (Bed-O-Cob) bedding. Animals had unrestricted access to food and water and were maintained in a temperature-controlled colony room on a 12-h:12-h light:dark cycle. All procedures were conducted in accordance with policy guidelines set by the National Institutes of Health and were approved by the Emory University Institutional Animal Care and Use Committee.

Plasmid design and construction

Design of the lentivirus encoding GFP under the control of the CCK promoter has been described previously (Chhatwal et al. 2007). Briefly, an approximately 3-kb region of 5′ genomic DNA up to and including the translation initiation site (ATG) of the CCK promoter was subcloned into the lentivirus transfer vector, pCMV–GFP–U3Nhe (Naldini et al. 1996), replacing the CMV promoter, to now drive GFP expression. Viral production and purification were previously described in detail (Tiscornia et al. 2006). Briefly, recombinant lentiviruses were produced by transient cotransfection of HEK293T cells with the expression vector, the packaging construct Δ8.9 (pCMV-Δ8.9), and the envelope plasmid encoding vesicular stomatitis virus G (VSV-G; pCMV-VSV-G) using the calcium-phosphate method. Virus supernatants were collected 2 and 4 days after transfection and stored on ice until processed. Supernatant was centrifuged at 5,000 rpm for 15 min, filtered through a 0.8-μm filter, and then centrifuged at 27,000 rpm for 90 min. The viral pellets were resuspended in phosphate-buffered saline (PBS) with 1% bovine serum albumin to yield a titer of 5.0×10^8–1.0×10^9 infectious U/ml, based on expression analyses with infected HEK293 cells following serial dilutions of concentrated virus.

Surgical procedures and virus infusions

For virus infusions, animals were anesthetized deeply with a ketamine/dormitor cocktail and placed in a stereotaxic instrument. Stereotaxic coordinates for the juvenile rat basolateral amygdala were determined empirically and based on the *Rat Brain Atlas* (Paxinos and Watson 2005). Coordinates were 2.0 mm posterior and ±4.5 mm lateral to bregma and 8.4 mm below bregma. The head was positioned in the stereotaxic frame so that the skull was level between lambda and bregma. Bilateral infusions of the CCK–GFP lentivirus were delivered over a 10-min period through a WPI Nanofil syringe with a 35-gauge beveled needle (World Precision Instruments [WPI], Sarasota, FL). A total of 2 μl/side was infused at a rate of 0.2 μl/min. The injection needle was left in place for an additional 5 min following infusions to allow for diffusion of the virus. All rats were returned to their home cages and allowed to recover for ≥14 days before electrophysiological experiments began.

Electrophysiological studies

PREPARATION OF ACUTE SLICES FROM THE BLA. To obtain slices from the BLA, rats were decapitated under isoflurane anesthesia (Abbott Laboratories, North Chicago, IL). The brains were rapidly removed and placed in ice-cold kynurenic acid–based artificial cerebrospinal fluid (KA-ACSF), which contained (in mM): NaCl (130), KCl (3.5), KH_2PO_4 (1.1), $MgCl_2$ (6.0), $CaCl_2$ (1.0), $NaHCO_3$ (30), glucose (10), and kynurenic acid (2). The glutamatergic antagonist kynurenic acid was included in the KA-ACSF to suppress any unwanted effects of glutamate release that may occur during tissue slicing. A block of tissue containing the BLA was then mounted on the chuck of a Leica VTS-1000 vibrating microtome (Leica Microsystems, Wetzlar, Germany) and 350-μm coronal slices were cut. Slices were then hemisected and hand-trimmed to remove excess tissue dorsal to the amygdala. Slices were transferred to a holding chamber containing KA-ACSF at 32°C and gassed with a 95% O_2-5% CO_2 mixture for ≥40 min before being placed in oxygenated regular ACSF (ACSF) at room temperature, containing (in mM): NaCl (130), KCl (3.5), KH_2PO_4 (1.1), $MgCl_2$ (1.3), $CaCl_2$ (2.5), $NaHCO_3$ (30), and glucose (10). Experiments were started a minimum of 30 min after the transfer of slices into ACSF.

For recording, slices were placed in a Warner Series 20 recording chamber (Warner Instruments, Hamden, CT) mounted on the fixed stage of a Leica DM-LFS microscope (Leica Microsystems). Slices were fully submerged and continuously perfused at a rate of 1–2 ml/min with heated (32°C) and oxygenated ACSF. GFP^+ neurons were selected under fluorescent illumination with a ×40 water-immersion objective. Images were captured with a Hamamatsu Orca ER CCD camera (Hamamatsu, Tokyo) controlled by SimplePCI software (Compix, Sewickley, PA). The selected cells were then visualized with infrared illumination and targeted for recordings. Whole cell patch-clamp recordings were conducted using thin-walled borosilicate glass-patch electrodes (WPI) that were pulled on a P-97 Flaming/Brown micropipette puller (Sutter Instruments, Novato, CA). Patch electrodes had resistances ranging from 4 to 7 MΩ when filled with standard patch solution that contained (in mM): K-gluconate (138), KCl (2), $MgCl_2$ (3), phosphocreatine (5), K-ATP (2), NaGTP (0.2), HEPES (10), and biocytin/neurobiotin (3 mg/ml). The patch solution was adjusted to a pH of 7.3 with KOH and had a final

osmolarity of 280 mOsm. Recordings were obtained using an Axopatch-1D amplifier (Molecular Devices, Sunnyvale, CA), a Digidata 1320A A/D interface, and pClamp 9 software (Molecular Devices). For all experiments, whole cell patch-clamp configuration was established and cell responses were recorded in current-clamp mode with data filtered at 5 kHz and a sampling rate of 10 kHz. Whole cell access resistances were in the range 5–25 MΩ and were monitored during the course of each experiment. Neurons were excluded from analysis if their resting membrane potential (V_m) was more positive than −55 mV and/or if their action potentials did not surpass +5 mV. A standard series of current-clamp test protocols were conducted to determine the physiological characteristics of each neuron at a holding potential of −60 mV. The passive and active membrane properties of each neuron were primarily assessed by determining the voltage response to transient (750-ms) incremental current steps ranging from −250 to +200 pA. The incremental current varied from cell to cell; however, a standard increment was used for each individual cell.

ELECTROPHYSIOLOGICAL PARAMETER DEFINITIONS. *Fast afterhyperpolarization (fAHP, in mV).* The difference between the action potential threshold and the most negative membrane potential attained after the action potential, measured in response to the smallest depolarizing current step (10 ms) evoking an action potential.

Medium afterhyperpolarization (mAHP, in mV). The difference between baseline (−60 mV) and the most negative membrane potential after a 750-ms depolarizing current injection, measured on the highest current step achieved that produced at least one action potential and measured within 100 ms of the offset of the current injection as defined by Schwindt et al. (1988).

Input resistance (R_{in}, in MΩ). The difference between baseline (−60 mV) and the peak voltage response divided by the injected current.

Membrane time constant (τ, in ms). Determined from the monoexponential curve best fitting the voltage deflection evoked in response to a −5-pA hyperpolarizing current step.

Resting membrane potential (V_m, in mV). The steady-state membrane potential reached a few minutes after breaking the seal, with no DC current applied.

First interspike interval (ISI_1, in ms). The time interval between the threshold of the first action potential and the threshold of the second action potential in response to a 750-ms depolarizing current injection.

Last interspike interval (ISI_{last}, in ms). The time interval between the threshold of the penultimate action potential and the threshold of the last action potential in response to a 750-ms depolarizing current injection.

Spike adaptation ratio (dimensionless). The ratio of ISI_1 to ISI_{last}.

Sag ratio (dimensionless). The difference between the steady-state membrane potential at the end of a 750-ms hyperpolarizing current step and the most negative membrane potential at the beginning of the step, divided by the most negative membrane potential.

Rectification ratio (dimensionless). The difference between the peak membrane potentials at the beginning of the two smallest hyperpolarizing steps divided by the difference between the peak membrane potentials at the beginning of the two largest hyperpolarizing steps, such that a cell with no observable inward rectification has a rectification ratio equal to 1.

Spike threshold (in mV). The point at which the action potential was initiated. The point at which the membrane potential showed a >10-fold change in the rate of rise (mV/ms) in response to the smallest depolarizing current step (10 ms) evoking an action potential.

Spike amplitude (in mV). The difference between the threshold and the voltage at the peak of the action potential.

Spike half-width (in ms). Measured at half-height between threshold and peak action potential.

10–90% rise time (in ms). Time to reach 90% of the peak amplitude of the action potential from 10% of the peak amplitude during the upswing of the action potential.

90–10% decay time (in ms). Time to reach 10% of the peak amplitude of the action potential from 90% of the peak amplitude during the downswing of the action potential.

Instantaneous firing frequency (in Hz). The reciprocal of the interspike interval (in ms) multiplied by 1,000.

MORPHOLOGICAL RECONSTRUCTIONS OF RECORDED NEURONS. Following recordings, slices were fixed overnight in 4% paraformaldehyde in 0.1 M PBS and then transferred to cryoprotectant (25% glycerine, 20% dH_2O, 30% ethylene glycol, 25% 0.2 M phosphate buffer). Slices (350 μm) were resectioned to 70 μm on a freezing microtome, rinsed in 0.1 M PBS, and permeabilized for 1 h in 0.5% Triton X-100 in 0.1 M PBS. To neutralize endogenous peroxidases, sections were incubated in 0.3% H_2O_2 for 30 min and then incubated in Elite ABC Reagent (Vector Laboratories) for 1.5 h at room temperature. Biocytin-filled neurons were visualized with nickel-intensified 3,3′-diaminobenzidine-4HCl (DAB; Sigma), rinsed with 0.1 M PB, mounted on gel-subbed slides, and allowed to air dry overnight. Sections were dehydrated in an ethanol series, cleared with xylene, and coverslipped with Permount (Fisher Scientific). Some biocytin-filled neurons were alternatively visualized using Alexa568-conjugated streptavidin (1:500; Molecular Probes, Eugene, OR). Biocytin-filled neurons were traced and digitally reconstructed using Neurolucida 7 (MicroBrightField) with a ×40 objective on an Olympus BX51 microscope.

Cell culture and immunocytochemistry

Adult amygdala primary cell cultures were obtained as previously described (Brewer and Torricelli 2007). Briefly, amygdala from rats were rapidly dissected in Hibernate-A (BrainBits, Springlield, IL)/B27 and glutamax (Invitrogen, Carlsbad, CA) at 4°C, then sliced into 500-μm sections and incubated at 30°C for 8 min while shaking. Tissue was then incubated in Hibernate-A/Papain (6 mg/ml) at 30°C for 30 min, shaking at 170 rpm. Slices were then triturated and centrifuged through an OptiPrep density gradient, resuspended in Hibernate-A/B27, and plated in a 24-well plate on poly-D-lysine (Sigma) coated coverslips at a concentration of 320 cells/mm^2. After 7 days in vitro cells were infected with the CCK–GFP lentivirus. Three days after infection, cells were fixed with 4% paraformaldehyde for 20 min, rinsed three times with 0.1 M PBS, and incubated for 1 h in normal goat serum with 0.5% Triton X-100. Cells were then incubated for 48 h at 4°C with anti-GFP mouse IgG (1:1,000; Invitrogen) and anti-CCK8 rabbit IgG (1:1,000; Sigma), and then rinsed three times with PBS and incubated with AlexaFluor 488 goat anti-mouse IgG (for GFP) and AlexaFluor 594 goat anti-rabbit IgG (for CCK8) for 1 h at room temperature. Cells were then rinsed three times with PBS and incubated with Hoechst 33342 (1:1,000) for 10 min at room temperature and rinsed a final three times. Cells were imaged on a Nikon Eclipse TE3000 inverted microscope with NIS Elements (Nikon) software.

Fluorescent in situ hybridization

Rats were infused with the CCK–GFP lentivirus as described earlier (surgical procedures and virus infusions) and allowed to recover for ≥14 days. Animals were anesthetized and decapitated and brains were rapidly removed, frozen on dry ice, and stored at −80°C until processing. Fresh-frozen tissue was sectioned at 30 μm on a cryostat, mounted on Superfrost Plus slides (Fisher Scientific), and allowed to air dry. Hybridization procedures were previously described in detail (Ressler et al. 2002), with slight modifications. Briefly, cDNA clones containing the coding sequence of the mouse gene for CCK and the coding sequence for GFP–WPRE were linearized with appropriate restriction enzymes. Fluorescently labeled riboprobes were generated with T3 (CCK) or T7 (GFP–WPRE) RNA polymerase (Promega Riboprobe Combination System). The CCK

riboprobe was labeled with digoxigenin (DIG) and the GFP–WPRE riboprobe was labeled with fluorescein. Following a prehybridization procedure, the sections were hybridized with both riboprobes at 55°C for 16 h and then subjected to a series of stringent washes. Sections were then incubated with anti-fluorescein-POD, Fab fragments, followed by fluorescent amplification and peroxidase quenching, and then with anti-digoxigenin-POD, Fab fragments (Roche). Signals were amplified with the TSA Plus Fluorescein Fluorescence System or TSA Plus Cy3 Fluorescence System (PerkinElmer) following each series of primary antibodies. Sections were coverslipped with Hard Set antifade mounting medium (Vector Laboratories).

Statistical analysis

Statistical analyses were carried out using SPSS 15.0 (SPSS, Chicago, IL). An unsupervised, hierarchical cluster analysis using Ward's method (Ward Jr 1963) and squared Euclidian distance was performed to classify subtypes of CCK^+ cells in the BLA. This method has been used successfully by previous studies to classify somatostatin cells of the sensorimotor cortex and projection neurons and interneurons of the lateral amygdala (Halabisky et al. 2006; Sosulina et al. 2006). Briefly, this clustering method begins by separating each individual neuron into a cluster by itself. At each stage of the analysis, the neurons that are most similar, as measured by our electrophysiological parameters, are grouped together to form another larger cluster. This process continues until all of the neurons are joined into a single cluster. Ward's method minimizes the error sum of squares of any pair of clusters formed at a given step; this maximizes between-group differences and minimizes within-group differences. Before clustering, each electrophysiological property was log-transformed and converted into standardized z-scores. This achieves a normal distribution and prevents variables with larger ranges from having a greater influence on the cluster solution than variables with small ranges. After the hierarchical cluster analysis was performed, the appropriate number of clusters was determined by examining within-group and between-group squared Euclidian distances. A good cluster solution should have large between-cluster differences and small within-cluster differences. A one-way ANOVA was used to detect statistically significant differences in electrophysiological parameters among the reported clusters. For all analyses, statistical significance was ascribed at $P < 0.05$.

The parameters used in the cluster analysis were chosen based on their lack of linear correlation with each other determined by a correlation analysis among all variables. Membrane time constant (τ) was removed because of its linear correlation with R_{in}. Likewise, ISI_1 and ISI_{last} were removed because of their correlation with spike adaptation ratio. Finally, 10–90% rise time and 90–10% decay time were removed from the analysis because they were highly correlated with each other and spike half-width. This left R_{in}, spike adaptation ratio, rectification ratio, sag ratio, resting membrane potential, spike threshold, spike amplitude, spike half-width, mAHP, and fAHP for the cluster analysis.

Further analysis was conducted using DFA to determine the electrophysiological properties most strongly contributing to group membership. In addition, DFA builds a predictive model for group membership. Briefly, this analysis attempts to find linear combinations of the variables that best separate the groups of cells by maximizing the between-group variance. Finally, a leave-one-out cross-validation procedure was then used to validate the discriminant functions.

RESULTS

CCK–GFP lentivirus specifically labels CCK-expressing interneurons

We generated two lentiviruses expressing either Cre-Recombinase or GFP under the control of an approximately 3-kb region of the CCK promoter and demonstrated highly specific expression of these lentiviruses in CA1, CA3, and dentate gyrus regions of the hippocampus (Chhatwal et al. 2007), which mirror CCK mRNA expression within these regions (Fig. 1). Here, we further demonstrated that GFP expression driven by the CCK promoter lentivirus is restricted to CCK^+ cells of the BLA (Fig. 2). Thus in amygdala adult primary cell culture we observed extensive colocalization of CCK and GFP when cultures were infected with the CCK–GFP virus (Fig. 2, *A–D*). Importantly, staining for GFP was absent in cells that did not also stain for CCK. Additionally, using dual-fluorescent in situ hybridization we show extensive colocalization of GFP–WPRE mRNA (to detect the presence of the CCK-promoter lentivirus) and CCK mRNA in neurons within the BLA of rats injected with the CCK–GFP lentivirus (Fig. 2, *E–J*). Notably, there is no expression of GFP–WPRE mRNA in cells that do not also express CCK mRNA in the BLA, demonstrating the specificity of GFP expression driven by our CCK promoter. Therefore we refer to GFP-positive cells as CCK^+ neurons. The CCK^+-labeled cells were multipolar, bipolar, or bitufted neurons with an average cell body area of 150.4 ± 31.0 μm^2 (Fig. 3). They either had medium- or

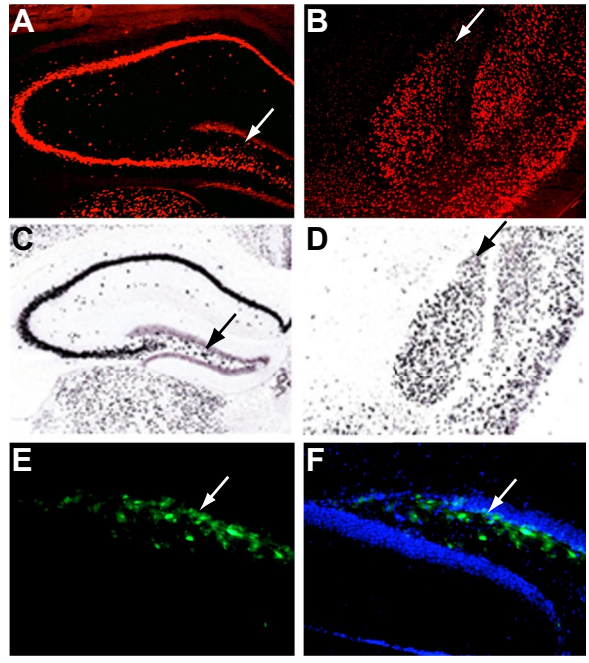

FIG. 1. Cholecystokinin (CCK) mRNA expression and lentiviral vector (LV)–CCK–green fluorescent protein (GFP) expression. CCK mRNA was examined using fluorescent in situ hybridization (FISH). A high level of expression was observed in the hippocampus (*A*) and in the basolateral complex of the amygdala (*B*). This expression recapitulates the expression observed within the same areas in the Allen Brain Atlas (*C*, *D*). Arrows (*A*, *C*) indicate the interneuron-rich region separating the polymorphic cell layer of the dentate gyrus, which expresses CCK mRNA, whereas the granule cell layer lacks CCK mRNA. Arrows (*B*, *D*) indicate the basolateral complex of the amygdala. This is also observed when the LV–CCK–GFP virus is used to infect the dentate gyrus (*E*, *F*) of rats (2 μl/injection), in which cells of the interneuron-rich region express GFP, whereas the granule cell layer of the dentate gyrus does not. *E*: GFP expression in the interneuron-rich region. *F*: photomicrograph showing combined Hoechst and GFP staining in the interneuron-rich region and the granule cell layer of the dentate gyrus.

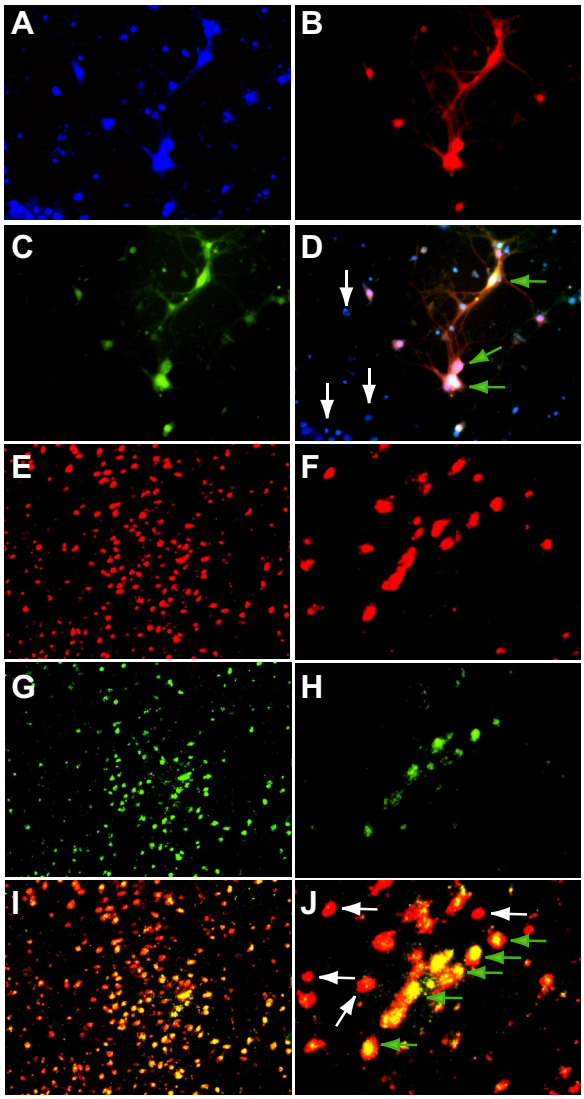

FIG. 2. Immunocytochemical verification of CCK^+ neurons in cultured amygdala neurons infected with the LV–CCK–GFP virus. *A*: Hoechst staining of primary neurons (blue). *B*: anti-CCK immunocytochemical staining (red). *C*: anti-GFP immunocytochemical staining (green). *D*: combined image demonstrating overlap of GFP expression with CCK and Hoechst staining. White arrows indicate cells that do not express CCK or GFP; green arrows indicate examples of triple-stained cells. *E–J*: dual FISH for CCK mRNA and the wPRE–GFP virus fragment mRNA in brains of infected rats. *E*: ×10 image of CCK mRNA within the basolateral amygdala (BLA). *G*: ×10 image of wPRE–GFP mRNA within the BLA. *I*: ×10 image of CCK mRNA and wPRE mRNA within the BLA. Red cells express CCK mRNA only; yellow cells express both wPRE mRNA and CCK mRNA. *F*: ×20 image of CCK mRNA. *H*: ×20 image of wPRE–GFP mRNA within the BLA. *J*: ×20 image demonstrating colocalization of CCK mRNA and wPRE–GFP mRNA in the same cells. Red cells express CCK mRNA only; yellow cells express both wPRE mRNA and CCK mRNA. White arrows indicate cells expressing CCK mRNA alone; green arrows indicate cells expressing CCK mRNA and wPRE–GFP mRNA. No cells expressed wPRE–GFP mRNA alone. We demonstrate excellent colocalization of CCK mRNA and wPRE–GFP expression within the BLA, indicating specificity of the CCK promoter virus.

spine-sparse dendrites (Fig. 3), which is in agreement with a previous immunocytochemical study describing CCK neurons of the BLA (Mascagni and McDonald 2003). Taken together, these data demonstrate highly specific expression of GFP within the appropriate subpopulation of cells in the BLA.

Three electrophysiologically distinct CCK^+ subtypes in the BLA

Previous studies have reported considerable heterogeneity in the electrophysiological properties of cortical CCK^+ and SOM^+ neurons, as well as subcortical GABAergic neurons (Halabisky et al. 2006; Hammack et al. 2007; Kawaguchi and Kondo 2002; Kawaguchi and Kubota 1998; Ma et al. 2006; Sosulina et al. 2006), although it remains unclear whether CCK^+ neurons of the BLA consist of more than one subtype. To address this question with a hypothesis-neutral approach, we recorded the electrophysiological properties of identified CCK^+ interneurons within the BLA in whole cell current-clamp mode and used the electrophysiological variables to identify possible subtypes using an unsupervised method of cluster analysis (hierarchical cluster analysis). A total of 57 neurons had data on all variables and were used in the cluster analysis. Membrane time constant (τ), ISI_1, ISI_{last}, 10–90% rise time, and 90–10% decay time were removed from the analysis because they were highly correlated with other variables (see *Statistical analysis*) and this would skew results of the cluster analysis. This analysis yielded a dendrogram (Fig. 4), which shows the squared Euclidian distance between group centroids of each merged cluster. Results from analysis of within-group and between-group squared Euclidian distances identified three clusters of CCK^+ neurons corresponding to branches 1, 2, and 3 in Fig. 4. We have defined these branches as CCK^+ Type I, Type II, and Type III neurons. An ANOVA was run to identify significant differences in electrophysiological properties among the cell types and to further validate the clustering algorithm. The electrophysiological properties of each group are shown in Table 1. In addition, to further verify that the cells we recorded from were interneurons, we also recorded the electrophysiological properties of 13 pyramidal neurons; these neurons were identified by their large soma and low input resistance (~59 MΩ) that were chosen at random within the BLA and compared with the CCK^+ interneurons.

The three distinct CCK^+ subtypes (Type I–Type III) were clearly distinct from BLA pyramidal neurons (PN) (Table 1). In agreement with the morphological classification of L and S CCK neurons, input resistance was a major factor in determining group membership among the CCK^+ cells. Type III CCK^+ neurons had the highest input resistance (521 ± 91 MΩ, Table 1), which was significantly different from that of all the other CCK^+ cell types [$F_{(3,69)} = 23.3$ $P < 0.05$], and likely represent the previously identified type S CCK cells (Mascagni and McDonald 2003). CCK^+ Type I and Type II neurons likely represent the type L cells previously identified. All CCK^+ subtypes had significantly greater input resistances compared with those of pyramidal neurons [$F_{(3,69)} = 23.3$ $P < 0.05$, Table 1]. These data partially confirm that we were recording only from interneurons and likely only from CCK^+ cells. In our recording environment, pyramidal neurons typically have input resistances between 40 and 70 MΩ, whereas interneurons have input resistances >100 MΩ (Table 1). There were no significant differences found among the three CCK^+ subtypes in the time constant for membrane charging (tau), last interspike interval (ISI_{last}), 10–90% rise time, or 90–10% decay time ($P > 0.05$, Table 1).

On further analysis of spike frequency adaptation and instantaneous firing frequency, it became apparent that Type

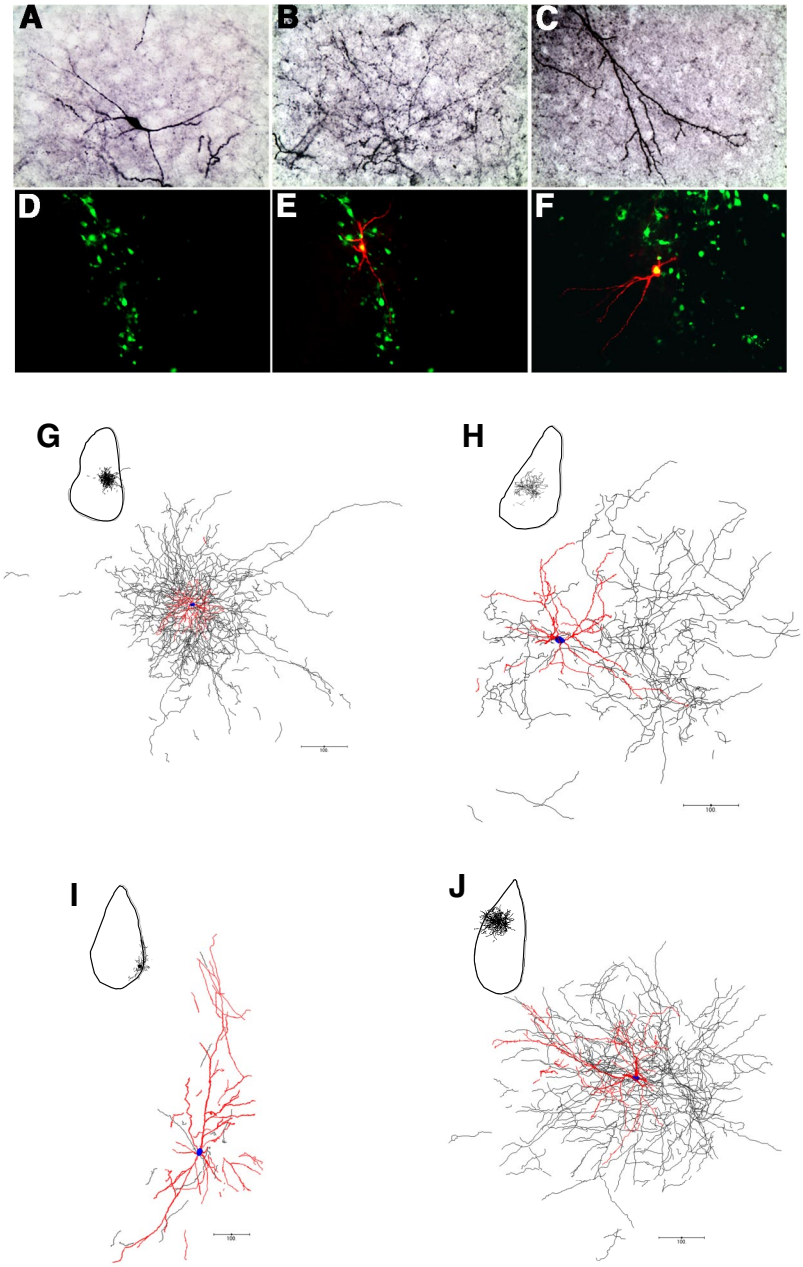

FIG. 3. Morphological properties of biocytin-filled CCK^+ neurons in the BLA. *A–C*: CCK^+ neurons were filled with biocytin during electrophysiological recording and then visualized using 3,3′-diaminobenzidine-4HCl (DAB). The labeled cells were multipolar, bipolar, or bitufted neurons with an average cell body area of 150.4 ± 31.0 μm^2 and had medium or spine-sparse dendrites (*A*, *C*). The axonal arborizations of the CCK^+ neurons could be quite extensive (*B*). *D*: GFP expression in GFP^+/CCK^+ neurons of the BLA. *E–F*: combined images of GFP fluorescence within the BLA and neurons that were filled with biocytin and visualized using AlexaFluor 568 conjugate. *G–J*: typical morphological reconstructions of GFP^+/CCK^+ interneurons in the BLA using Neurolucida. *Insets* show the location of the cells within the BLA. Cell bodies are shown in blue, dendrites are shown in red, and axons are shown in gray. The axonal arborizations of the neurons could be quite extensive and were also observed to extend medially or laterally out of the BLA, as can be seen in *G* and *J*.

II CCK^+ neurons could be further segregated into two types based on their rates of spike frequency adaptation. This was done by creating a cutoff of 50 Hz for the instantaneous firing frequency for the first interspike interval. CCK^+ Type II neurons are subdivided into an adapting subgroup (Type II Ad, >50 Hz) and a nonadapting subgroup (Type II NAd, <50 Hz) (Figs. 4 and 5). Type II Ad neurons exhibited an initial burst-firing pattern (91 Hz), but then quickly settled into a more regular firing pattern. Type II NAd neurons exhibited a more regular firing pattern (~20 Hz) that was similar to the firing pattern exhibited by Type I and Type III neurons (~20–30 Hz) (Fig. 5). The firing frequency of Type II Ad neurons was significantly greater than that of all other cell types for the first interval ($P < 0.05$), greater than that of Type II NAd and Type I for the second interval ($P < 0.05$), and greater than that of Type II NAd neurons for the first six intervals ($P < 0.05$; Fig. 5). Given this difference between Type II Ad and Type II NAd neurons, we also compared the rest of their electrophysiological parameters. Type II Ad neurons had a significantly shorter ISI_1 compared with that of Type II NAd ($P < 0.05$, 13.3 ± 1.3 vs. 47.4 ± 5.4 ms, respectively) and had a significantly lower spike adaptation ratio ($P < 0.05$, 0.19 ± 0.05 vs. 0.41 ± 0.042, respectively). Type II Ad and Type II NAd neurons did not differ significantly on the remaining electrophysiological parameters. This can also be seen in the way Type II Ad and Type II NAd are intermixed in the dendrogram from the cluster analysis (Fig. 4). Additionally, Type II Ad neurons had a significantly shorter ISI_1 compared with that of all cell types [$F_{(4,69)} = 14.1$, $P < 0.05$] and a significantly lower spike adaptation ratio [$F_{(4,69)} = 12.0$, $P < 0.05$].

Single action potentials generated in response to a 10-ms suprathreshold depolarizing current injection also differed

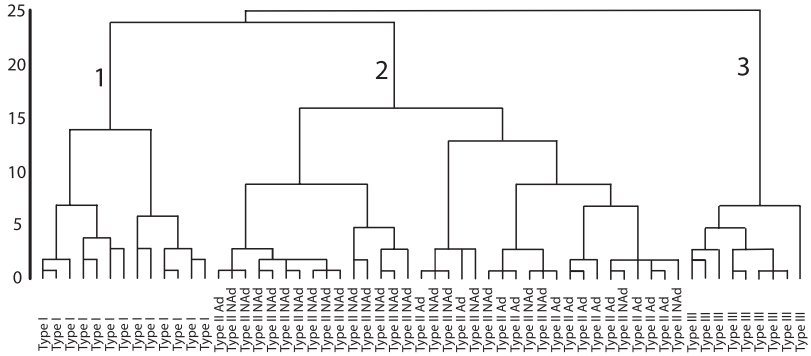

FIG. 4. A dendrogram illustrating the results from a hierarchical cluster analysis. Intersection of the dendrogram branches with the *x*-axis represents individual neurons. The *y*-axis is the squared Euclidian distance between group centroids at each branch point. Longer vertical lines indicate greater distance. Three groups were determined by analysis of within- and between-group distances, corresponding to branches 1, 2, and 3. These branches correspond to CCK^+ Type I, Type II, and Type III neurons. The individual cells are coded into their respective groups along the *x*-axis. Type II CCK^+ neurons could be further separated based on their firing rates into adapting (Type II Ad) and nonadapting (Type II NAd) neurons.

somewhat among the CCK^+ subtypes. Thus Type III neurons had a significantly larger fAHP compared with that of Type II CCK^+ neurons, but did not differ from Type I neurons [$F_{(4,69)} = 3.7$, $P < 0.05$, Fig. 6*C*, Table 1]. Type III neurons also had a significantly more depolarized action potential threshold compared with that of all other CCK^+ subtypes [$F_{(4,69)} = 3.9$, $P < 0.05$]. Action potential half-widths did not differ among the CCK^+ cell types, although all CCK^+ cell types had significantly longer action potential half-widths compared with those of pyramidal neurons [$F_{(4,69)} = 3.3$, $P < 0.05$, Table 1]. Finally, Type II neurons exhibited a significantly greater action potential amplitude compared with that of Type I and Type III neurons [$F_{(4,69)} = 11$, $P < 0.05$, Table 1]. Type III neurons exhibited the smallest action potential amplitude compared with that of the other CCK^+ cell types. No differences were found in rise time and decay time among the three CCK^+ subtypes (Table 1). Finally, Type I neurons exhibited a significantly smaller mAHP compared with that of both Type II and Type III neurons [$F_{(4,69)} = 5.6$, $P < 0.05$, Table 1]. The size of the mAHP did not correlate with the size of the fAHP.

In response to transient (750-ms) hyperpolarizing current injection, Type III CCK^+ neurons exhibited a prominent depolarizing sag in their voltage response that was both time and voltage dependent and was likely mediated by the hyperpolarization-activated cationic current, I_h (Fig. 6*D*). Type III neurons also displayed a "rebound" depolarizing potential on the offset of the hyperpolarizing current step (Fig. 6*D*). The depolarizing sag displayed by Type III neurons was significantly greater than the sag exhibited by Type I and Type II CCK^+ subtypes, as measured by the sag ratio [$F_{(4,69)} = 10.5$, $P < 0.05$, Fig. 6*D*, Table 1 (sag ratio)]. In contrast, Type I neurons displayed little depolarizing sag in their voltage response to hyperpolarizing current injection (Fig. 6*D*, Table 1). Type I and Type II neurons displayed a fast time-independent rectification that was significantly greater than the rectification exhibited by Type III neurons [$F_{(4,69)} = 4.0$, $P < 0.05$, Fig. 6*D*, Table 1]. This fast rectification was most likely due to activation of an inwardly rectifying potassium current (K_{IR}) because rectification increased with increasing levels of membrane hyperpolarization. It is important to note that pyramidal neurons were significantly different compared with at least one of the CCK^+ cell types on all electrophysiological properties except ISI_{last} (Table 1).

Multivariate analysis of CCK$^+$ subtypes

After calculating 15 electrophysiological properties for each of 57 neurons and using 10 of these properties to cluster the neurons into three subtypes (five of the variables were omitted because of linear correlation with each other; see METHODS), we determined which electrophysiological properties best discriminated among the three CCK^+ subtypes. In addition we wanted to be able to determine group membership of newly encountered cells without having to conduct additional cluster analysis. A DFA performed on cells previously classified by cluster analysis generates an algorithm that can be used to predict

TABLE 1. *Electrophysiological properties of CCK$^+$ and pyramidal neurons of the BLA*

Property	Type I (n = 13) 23%	Type II (n = 35) 61%	Type III (n = 9) 16%	Pyramidal Cells (n = 13)
R_{in}, MΩ* $P < 0.001$	280 ± 51^{3,PN}	230 ± 17^{3,PN}	521 ± 91^{1,2,PN}	59 ± 3.4^{1,2,3}
Tau, ms $P = 0.077$	18.8 ± 2.4^{3}	22.6 ± 1.5	29.3 ± 5.9^{1,PN}	17 ± 1.4^{3}
RMP, mV* $P < 0.001$	−68 ± 0.9^{2,3,PN}	−61 ± 0.9^{1}	−58 ± 0.7^{1}	−61 ± 0.8^{1}
ISI_1, ms* $P < 0.001$	39.8 ± 5.6^{PN}	32.4 ± 4.4^{3,PN}	62.9 ± 15.21^{2,PN}	13.4 ± 5.4^{1,2,3}
ISI_{last}, ms $P = 0.62$	77 ± 11.1^{2,3}	113 ± 9.3^{1}	138 ± 25.91	110.5 ± 30.7
Spike adaptation ratio* $P < 0.001$	0.56 ± 0.06^{2,PN}	0.29 ± 0.03^{1,PN}	0.45 ± 0.08^{PN}	0.19 ± 0.08^{1,2,3}
Sag ratio* $P < 0.001$	0.006 ± 0.001^{2,3,PN}	0.04 ± 0.006^{1,3,PN}	0.064 ± 0.01^{1,2}	0.062 ± 0.006^{1,2}
Rectification ratio* $P = 0.011$	1.68 ± 0.2^{3}	1.55 ± 0.06^{3,PN}	1.11 ± 0.07^{1,2}	1.27 ± 0.07^{2}
Medium AHP, mV* $P = 0.002$	1.4 ± 0.4^{2,3,PN}	2.2 ± 0.2^{1}	3.5 ± 0.8^{1}	3.4 ± 0.5^{1}
Fast AHP, mV* $P = 0.016$	12.4 ± 1.8	9.1 ± 1.0^{3}	16.1 ± 1.7^{2,PN}	6.9 ± 0.9^{3}
Threshold, mV* $P = 0.012$	−44 ± 1.1^{3}	−45 ± 0.7^{3}	−39 ± 1.5^{1,2,PN}	−43 ± 1.0^{3}
AP amplitude, mV* $P < 0.001$	75 ± 4.8^{2,3,PN}	85 ± 2.8^{1,3}	58 ± 4.6^{1,2,PN}	92.1 ± 2.9^{1,3}
AP half-width, ms* $P < 0.001$	1.03 ± 0.092^{PN}	1.06 ± 0.055^{PN}	1.01 ± 0.095^{PN}	0.74 ± 0.052^{1,2,3}
Rise time, ms $P = 0.052$	0.45 ± 0.044	0.46 ± 0.027^{PN}	0.47 ± 0.036^{PN}	0.33 ± 0.03^{2,3}
Decay time, ms* $P = 0.036$	0.89 ± 0.11	1.13 ± 0.18^{PN}	0.75 ± 0.06	0.62 ± 0.07^{2}

Values are means ± SE. Electrophysiological properties in bold are those used for clustering interneurons into subtypes. Asterisks (*) indicate a significant difference among cell types based on an ANOVA, $P < 0.05$ (P values indicated). Superscript following the SE indicates cell type differences based on Fisher's post hoc analysis, $P < 0.05$. 1, Type I; 2, Type II; 3, Type III; PN, pyramidal neuron.

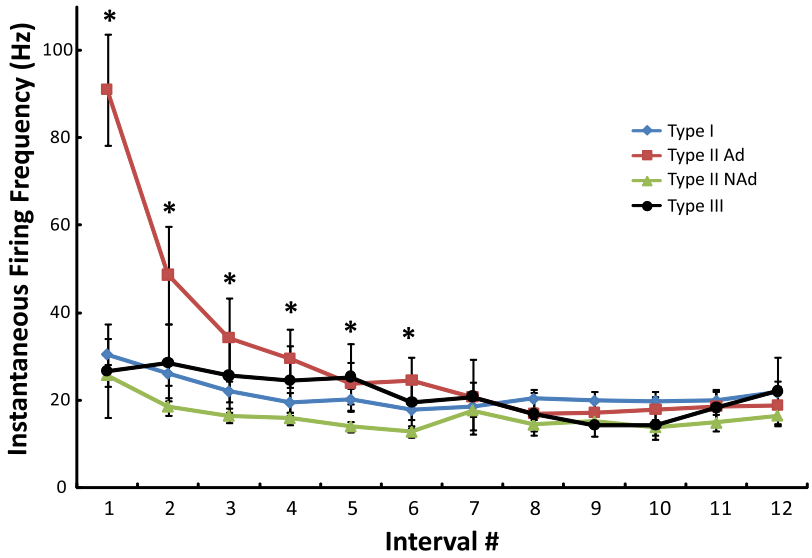

FIG. 5. Instantaneous firing frequency calculated from the interspike intervals (ISIs) of the first 12 action potentials generated in response to a 750-ms depolarizing current injection. Instantaneous firing frequency was calculated as 1/ISI. Type II cells could be further segregated into adapting (Type II Ad) and nonadapting (Type II NAd). Type II Ad neurons exhibited an initial burst-firing pattern (91 Hz) but then quickly settled into a more regular firing pattern. Type II NAd neurons exhibited a more regular firing pattern (~20 Hz) that was similar to the firing pattern exhibited by Type I and Type III neurons (~20–30 Hz). The firing frequency of Type II Ad neurons was significantly greater than that of all other cell types for the first interval ($P < 0.05$), greater than Type II NAd and Type I for the second interval ($P < 0.05$), and greater than Type II NAd neurons for the first 6 intervals ($P < 0.05$). Significant differences are denoted by asterisks (*).

group membership of newly encountered cells if all the same electrophysiological properties are known. Based on the 10 electrophysiological properties used to cluster the cells into three subtypes, we generated two discriminant functions. Both discriminant functions contributed significantly to group membership (Wilks' Lambda, $P < 0.001$, eigenvalues = 2.3 and 1.3, corresponding to 64 and 36% of the variance, respectively). The unstandardized discriminant function coefficients are depicted in Table 2 and the contribution of each variable to each discriminant function can be seen in the structure matrix (Table 3). Variables that are correlated with a particular discriminant function segregate cells most strongly along this function's axis relative to other functions. The first discriminant function distinguished cells based on sag ratio, resting membrane potential, mAHP, and rectification ratio (Table 3). The second function distinguished cells based on action potential (AP) amplitude, spike adaptation ratio, R_{in}, fAHP, and AP threshold. The discriminant scores for each cell were determined for discriminant functions 1 and 2, and demonstrate that there is good separation of all groups of CCK^+ cells in both discriminant functions, although the border between Type I and Type II NAd is slightly less well defined than the borders among all the other cell types (Fig. 7). To assess how well the discriminant functions work, we performed a leave-one-out cross-validation procedure (Halabisky et al. 2006). This procedure classifies each cell by the discriminant functions derived from all cases other than that case. If the procedure is not robust, then leaving out one cell will introduce errors in the classification. We found 90% of the cells to be correctly classified with this procedure, indicating that the discriminant functions, although not perfect, are very robust. Taken together, these data strongly suggest that electrophysiological properties alone can be used to classify CCK^+ neurons of the BLA into one of these three subtypes.

DISCUSSION

In the present study, we used a cell-type–specific promoter lentiviral vector driving GFP expression to visually identify CCK^+ cells of the BLA and record their physiological properties. Here, we report that CCK^+ interneurons of the BLA can be differentiated into three distinct electrophysiological subtypes (I, II, and III) based solely on their intrinsic membrane properties. We have previously demonstrated the high degree of specificity of the CCK promoter virus in vivo in the hippocampus (Chhatwal et al. 2007) and now demonstrate its specificity within the BLA. It is important to note the difference between CCK mRNA expression and CCK immunoreactive neurons in the BLA identified in a previous study (Mascagni and McDonald 2003). Fewer cells are identified using immunocytochemistry for protein versus in situ hybridization for CCK mRNA. There could be several reasons for this difference: *1*) Many more cells have the potential to produce CCK, but do not express the mature peptide at any given time. For example, CCK mRNA has been localized to glutamatergic projection neurons of the amygdala (Sosulina et al. 2006; Sugino et al. 2006), but is thought to be specific to GABAergic interneurons. *2*) There are more posttranscriptional or posttranslational variants of the mature peptide that are not recognized by the antibody used in the previous study. *3*) The mature peptide is rapidly transported to axon terminals, leading to low levels of detection in cell bodies. Notably, our CCK in situ hybridization results are identical to the Allen Brain Atlas expression of CCK mRNA (Fig. 1). The reason for the difference in CCK expression using the two techniques needs to be addressed, but is beyond the scope of the present study.

Although there is no agreement on what is required for a population of neurons to be considered a subtype, physiological diversity of interneuron subpopulations is well established. For instance, at least three distinct interneuron classes have been identified in the frontal cortex (Kawaguchi and Kubota 1998), sensory motor cortex (Gupta et al. 2000), hippocampus (Pawelzik et al. 2002), and neostriatum (Kawaguchi 1993). In these studies, the primary criterion for determining differences among the subtypes was their action potential firing pattern. Furthermore, evidence suggests that CA1 pyramidal cells are supported by 16 distinct interneuron subtypes, which have been classified based on their afferent–efferent connections, expression of cell signaling proteins, and their intrinsic membrane properties (Markram et al. 2004; Somogyi and Klausberger 2005). Finally, transgenic mice expressing GFP under the control of the GAD67 promoter have enabled the identifi-

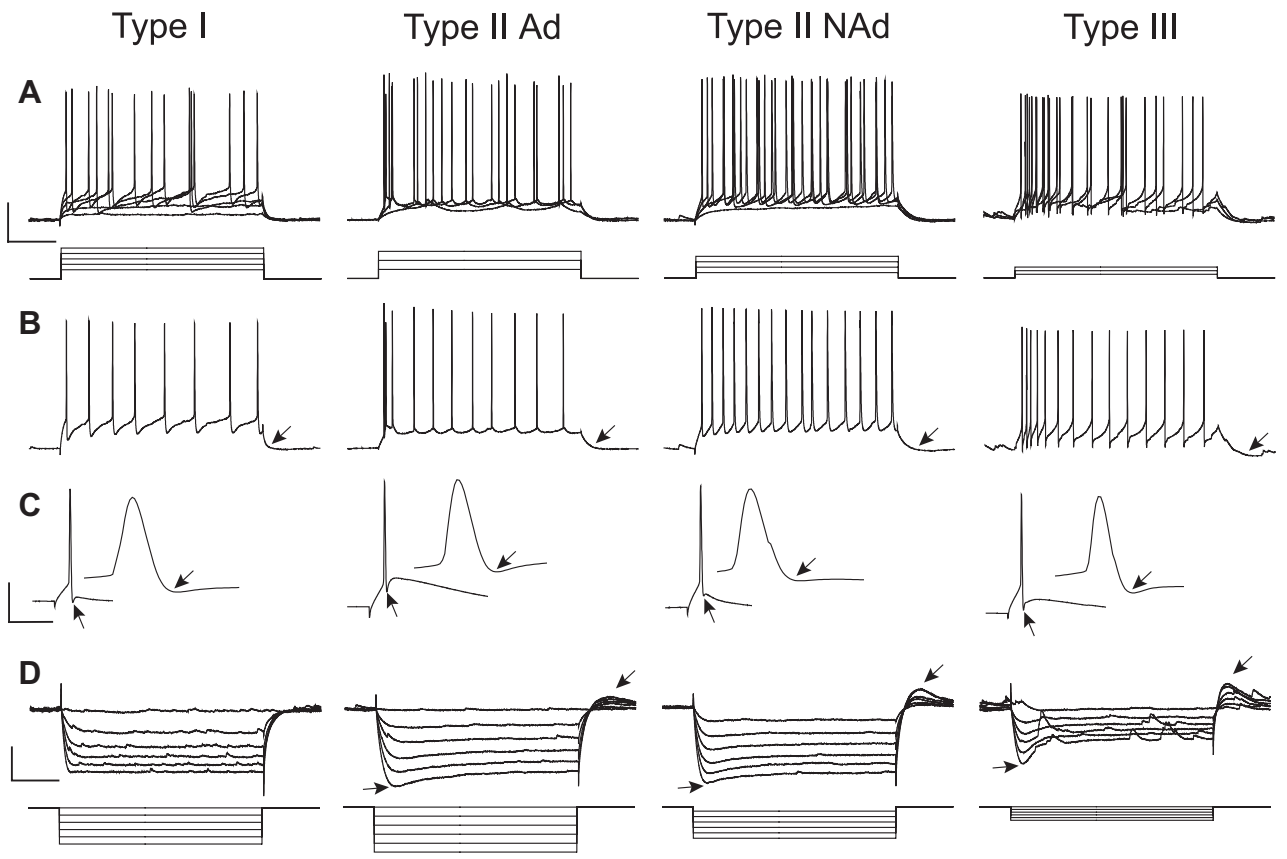

FIG. 6. Three physiologically distinct CCK^+ interneurons (Types I–III) identified through cluster analysis are found in the BLA, and differ in their response to depolarizing and hyperpolarizing current injection. Type II neurons were further segregated into Type II Ad and Type II NAd neurons based on their spike frequency adaptation. Type II Ad neurons exhibited an initial burst-firing pattern but then quickly settled into a more regular firing pattern. Type II NAd neurons exhibited a more regular firing pattern. *A*: responses to varying depolarizing current injection of Type I–Type III neurons; scale bars: 30 mV (225 pA); 200 ms (*B*) Type II Ad neurons responded to depolarizing current injection with an initial burst of action potentials that rapidly adapted. Type II NAd, Type I, and Type III neurons in general fired action potentials with a more regular firing pattern. Arrows in *B* indicate where the medium afterhyperpolarization (mAHP) was measured. *C*: single action potentials elicited by a 10-ms suprathreshold depolarizing current injection. Type III neurons exhibited a significantly larger fast afterhyperpolarization (fAHP) than that of the other subtypes. Scale bars: 30 mV; 30 ms. The *insets* are enlargements of the action potentials. Arrows in *C* indicate where the measurements for the fAHP were taken. *D*: responses to varying hyperpolarizing current injection. Type II and Type III neurons exhibited a depolarizing sag in response to hyperpolarizing current injection that was accompanied by a rebound depolarization on the offset of current injection (indicated by arrows); Type I neurons exhibit very little if any depolarizing sag in response to hyperpolarizing current injection. Scale bars: 10 mV (190 pA); 200 ms. Statistical differences for action potential firing patterns and single action potential properties are listed in Table 1.

cation of at least four distinct subtypes of SOM^+ interneurons in the cortex (Halabisky et al. 2006; Ma et al. 2006), based solely on their intrinsic membrane properties and action potential firing patterns.

Recently, laboratories—both ours and others'—have begun to classify subtypes of interneurons within the BLA. These studies suggest that interneurons of the BLA can be classified into at least four subtypes based on their intrinsic membrane properties, action potential firing patterns (Rainnie et al. 2006), and their calcium binding protein and neuropeptide expression (Mascagni and McDonald 2003; McDonald 1989; McDonald and Betette 2001; McDonald and Mascagni 2001a, 2002; McDonald and Pearson 1989; Muller et al. 2003). Moreover, PV^+ interneurons of the BLA can be further classified into two and perhaps four distinct subtypes based on their firing patterns and voltage responses to current injection (Meyer et al. 2002; Rainnie et al. 2006; Woodruff and Sah 2007b). Although quite different in organization and function from cortical structures, at least three distinct physiological cell types have also been identified within the bed nucleus of the stria terminalis (BNST) (Hammack et al. 2007), an area that largely contains GABAergic inhibitory neurons (McDonald 1983; Sun and Cassell 1993). Taken together, the current findings and data from previous findings suggest that there is more physiological and functional diversity among individual interneuron subtypes than previously thought.

Consistent with this hypothesis, a previous immunohistochemical study also suggested diversity among CCK^+ interneurons of the BLA based on morphological and cytochemical properties (Mascagni and McDonald 2003). In that study,

TABLE 2. *Unstandardized discriminant function coefficients*

Discriminant Function	R_{in}	Spike Freq. Adapt.	mAHP	fAHP	AP Half-Width	Rect. Ratio	Sag Ratio	RMP	AP Threshold	AP Spike Amp.
1	−0.654	−0.097	−0.378	0.430	0.397	0.263	−0.971	0.421	0.250	0.492
2	−0.195	−0.881	0.013	0.082	0.243	0.281	0.237	−0.328	0.225	0.801

TABLE 3. *Structure matrix coefficients*

Discriminant Function	R_{in}	Spike Freq. Adapt.	mAHP	fAHP	AP Half-Width	Rect. Ratio	Sag Ratio	RMP	AP Threshold	Spike Amp.
1	−0.279	0.104	−0.299*	−0.082	0.001	0.219*	−0.593*	0.435*	0.217	0.233
2	−0.411*	−0.537*	0.099	−0.344*	0.054*	0.199	0.480	−0.261	0.278*	0.491*

Pooled within-group correlations between discriminating variables and standardized canonical discriminant functions. An asterisk (*) indicates the largest correlation between each variable and any discriminant function. That variable contributes most to the segregation of cells along that function's axis, relative to other discriminant functions.

CCK^+ cells were segregated into two subtypes: *1*) type L (characterized by large soma) and *2*) type S (characterized by small soma). These CCK cells also exhibit neurochemical diversity in their expression of calcium-binding proteins and other neuropeptides. Whereas this analysis demonstrates morphological and neurochemical diversity among CCK interneurons, physiological/functional heterogeneity has not been established until recently. Here, we demonstrate that CCK cells of the BLA can be segregated into three physiologically distinct subtypes. In support of our classification, a previous report segregated CCK-expressing neurons into three of four total interneuron subtypes in the lateral amygdala (Sosulina et al. 2006). Furthermore, there is a possible correspondence between the previous morphological classification study (Mascagni and McDonald 2003) and the electrophysiological classification here, in that input resistance (R_{in}), which would be predicted to inversely correlate with soma size, was a major factor in determining group membership. Specifically, R_{in} separated Type III neurons from the rest of the CCK^+ subtypes and these cells may represent the type S CCK^+ cells because their R_{in} was significantly greater than that of all other CCK^+ subtypes. Type I and Type II cells likely represent the type L CCK^+ neurons. These data suggest that input resistance is a major factor contributing to the grouping of CCK^+ cells, but there are additional physiological variables that also contribute to their segregation.

Based on their action potential firing patterns, Type II cells could be further subdivided into two groups: those that display spike frequency adaptation (Type II Ad) and those that are nonadapting (Type II NAd, Fig. 5). Type I, Type II NAd, and Type III CCK^+ interneurons display little or no spike frequency adaptation. Importantly, the membrane properties of the CCK^+ neurons described in the present study are remarkably similar to those previously reported for CCK^+ interneurons of the BLA and cortex (Kawaguchi and Kubota 1998; Markram et al. 2004; Rainnie et al. 2006). Moreover, none of the CCK^+ interneurons recorded in this study resembled the "burst-firing" or "stutter-firing" PV^+ interneurons previously identified in the BLA (Rainnie et al. 2006). Consistent with immunohistochemical studies (Mascagni and McDonald 2003), these data suggest that visually identified CCK^+ BLA interneurons are physiologically distinct from the population of PV^+ interneurons, further validating the specificity of the CCK promoter lentivirus used in the present study.

Electrophysiological heterogeneity of CCK^+ interneurons of the BLA

The differences in electrophysiological properties observed among the CCK^+ cell types likely reflects heterogeneity in the expression of specific ion channels. The further segregation of Type II neurons into Type II Ad and Type II NAd based on their rates of spike frequency adaptation likely reflects differences in ion channel expression, regulating spike timing and interspike interval (e.g., SK, $K_v7.2/73$). Small-conductance Ca^{2+}-activated K^+ (SK) channels (SK1–SK3) and the voltage-gated K^+ channels, $K_v7.2/7.3$ that underlie the M-current (I_m), contribute to spike timing through modulation of the mAHP and interspike interval (Bond et al. 2005; Lawrence et al. 2006). Differences in SK and K_v7 channel expression might explain the differences in mAHP, spike frequency adaptation, and ISI_1 observed among the CCK^+ subtypes.

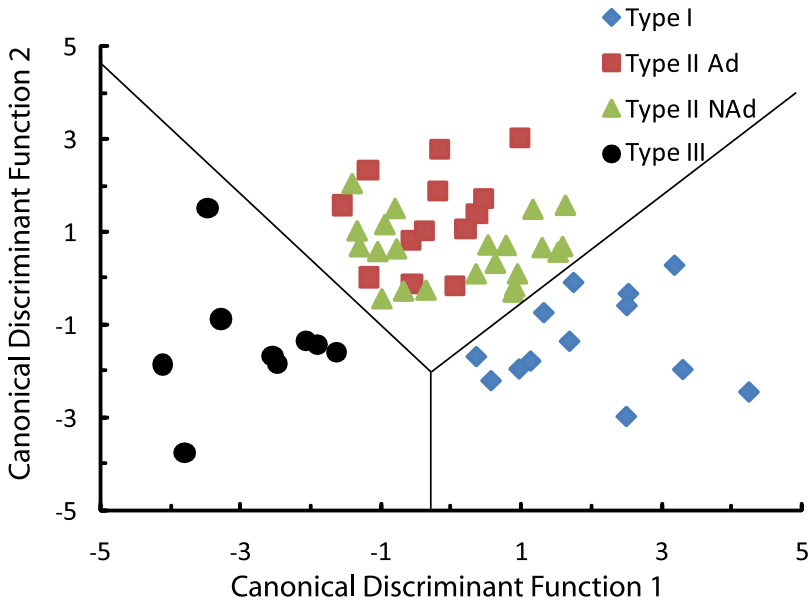

FIG. 7. Distribution of CCK^+ cells along canonical discriminant functions 1 and 2. There is good separation of the cells into three distinct groups along both discriminant functions. The first discriminant function distinguished cells based on sag ratio, resting membrane potential, mAHP, and rectification ratio. The second function distinguished cells based on action potential (AP) amplitude, spike adaptation ratio, R_{in}, fAHP, and AP threshold. Lines indicate boundaries between the territories occupied by each group.

In most cortical regions GABAergic interneurons can be distinguished from glutamatergic projection neurons by their comparatively short action potential duration and high firing rates (Beierlein et al. 2003; Gupta et al. 2000; McCormick et al. 1985). The short action potential duration has been attributed to selective expression of the voltage-gated potassium channels $K_v3.1$ and $K_v3.2$ in the interneuron population (Rudy and McBain 2001). It is thus notable that CCK^+ interneurons in the BLA exhibit relatively slow action potential durations, which were slower even than the action potentials exhibited by pyramidal neurons (Table 1), suggesting that these neurons show little or no expression of $K_v3.1$ and $K_v3.2$ channels. These data are consistent with the reported half-widths for regular-firing interneurons of the BLA, which have been identified as CCK neurons (Rainnie et al. 2006), as well as for CCK interneurons in the cortex (Kawaguchi and Kubota 1998). Moreover, a recent immunohistochemical study confirmed that CCK interneurons of the BLA do not express either $K_v3.1$ or $K_v3.2$ channels (McDonald and Mascagni 2006). Thus CCK interneurons of the BLA are similar to the CCK interneurons of the cortex in that they have relatively slow and, in some cases, adapting action potentials.

The results of the current study showing electrophysiologically distinct subgroups of CCK^+ interneurons provide additional evidence of functional differences and/or a division of labor within the CCK–BLA network. For example, a small population of type L CCK cells of the BLA expresses the $5\text{-}HT_{3A}$ serotonin receptor subtype (5-HT3AR) (Mascagni and McDonald 2007). Based on the present findings, we would predict that type L cells correspond to Type I and Type II cells, suggesting that 5-HT may exert its anxiolytic effects on fear and anxiety via modulation of GABA and CCK neurotransmission on this subset of CCK interneurons. Moreover, in the amygdala 53% of interneurons that express the 5-HT3 receptor also coexpress the CB1 subtype of cannabinoid receptor (Morales et al. 2004). In light of the fact that CB1 receptors are expressed predominantly by CCK interneurons in the BLA (Katona et al. 2001; McDonald and Mascagni 2001b), these data would further suggest that Type I and Type II CCK interneurons may preferentially express CB1 receptors. Significantly, activation of these CB1 receptors is necessary for the extinction of fear memories (Chhatwal et al. 2009). Thus selective activation of CB1 receptors in a subset of CCK interneurons may result in differential modulation of GABA and/or CCK release and thus modulate behavior.

Finally, many neurons of the CNS display an intrinsic resonance frequency at which the voltage response to current flow across the plasma membrane is maximal (Hutcheon et al. 1996a,b). The intrinsic resonance properties of a neuron confer the ability to oscillate at membrane potentials subthreshold for action potential generation and, consequently, these neurons have a preferential frequency at which they will respond most robustly to synaptic input. Significantly, BLA neurons display both subthreshold membrane oscillations and intrinsic resonance frequencies (Pape and Driesang 1998). Several factors determine the intrinsic resonance properties of a neuron, including its resting membrane input resistance (R_{in}). Thus Type I and Type II CCK interneurons would be predicted to differ significantly from Type III CCK interneurons in their intrinsic resonance frequency, as has been demonstrated in hippocampal interneurons (Pike et al. 2000). Moreover, Type II CCK neurons can be differentiated into adapting (Ad) and nonadapting (NAd) subtypes. Thus the same spike burst may be resonant for one cell, but not another (Izhikevich et al. 2003). In the present study we demonstrated that one subtype of CCK^+ cells (Type II Ad) exhibits initial bursts of action potentials followed by rapid spike frequency adaptation. As such, these cells might communicate with multiple postsynaptic cells at various resonance frequencies, thus having a wide range of influence on BLA network activity.

In summary, the CCK promoter virus is specific for CCK cells because of our previous characterization in the hippocampus (Chhatwal et al. 2007) and our characterization in the present study. Furthermore, the CCK^+ interneurons identified in the present study were physiologically and morphologically distinct from BLA pyramidal neurons, suggesting that we recorded from a distinct interneuron population within the BLA. Finally, the CCK^+ interneurons identified here had physiological characteristics highly consistent with previously identified CCK^+ neurons of the BLA and cortex. Thus we have identified three distinct subtypes of CCK interneurons within the BLA based on their electrophysiological properties.

GRANTS

This work was supported by National Institutes of Health Grants MH-069884, DA-019624, MH-069852, and MH-074097; the Center for Behavioral Neuroscience/National Science Foundation Agreement IBN-9876754; Burroughs Wellcome Fund; and National Center for Research Resources Base Grant P51-RR-000165 to Yerkes National Primate Research Center.

REFERENCES

Apergis-Schoute AM, Debiec J, Doyere V, LeDoux JE, Schafe GE. Auditory fear conditioning and long-term potentiation in the lateral amygdala require ERK/MAP kinase signaling in the auditory thalamus: a role for presynaptic plasticity in the fear system. *J Neurosci* 25: 5730–5739, 2005.

Beierlein M, Gibson JR, Connors BW. Two dynamically distinct inhibitory networks in layer 4 of the neocortex. *J Neurophysiol* 90: 2987–3000, 2003.

Belcheva I, Belcheva S, Petkov VV, Petkov VD. Asymmetry in behavioral responses to cholecystokinin microinjected into rat nucleus accumbens and amygdala. *Neuropharmacology* 33: 995–1002, 1994.

Bond CT, Maylie J, Adelman JP. SK channels in excitability, pacemaking and synaptic integration. *Curr Opin Neurobiol* 15: 305–311, 2005.

Brewer GJ, Torricelli JR. Isolation and culture of adult neurons and neurospheres. *Nat Protoc* 2: 1490–1498, 2007.

Campeau S, Davis M. Involvement of the central nucleus and basolateral complex of the amygdala in fear conditioning measured with fear-potentiated startle in rats trained concurrently with auditory and visual conditioned stimuli. *J Neurosci* 15: 2301–2311, 1995.

Campeau S, Miserendino MJ, Davis M. Intra-amygdala infusion of the N-methyl-D-aspartate receptor antagonist AP5 blocks acquisition but not expression of fear-potentiated startle to an auditory conditioned stimulus. *Behav Neurosci* 106: 569–574, 1992.

Chen Q, Nakajima A, Meacham C, Tang YP. Elevated cholecystokininergic tone constitutes an important molecular/neuronal mechanism for the expression of anxiety in the mouse. *Proc Natl Acad Sci USA* 103: 3881–3886, 2006.

Chhatwal JP, Gutman AR, Maguschak KA, Bowser ME, Yang Y, Davis M, Ressler KJ. Functional interactions between endocannabinoid and CCK neurotransmitter systems may be critical for extinction learning. *Neuropsychopharmacology* 34: 509–521, 2009.

Chhatwal JP, Hammack SE, Jasnow AM, Rainnie DG, Ressler KJ. Identification of cell-type specific promoters within the brain using lentiviral vectors. *Gene Ther* 14: 575–583, 2007.

Clugnet MC, LeDoux JE. Synaptic plasticity in fear conditioning circuits: induction of LTP in the lateral nucleus of the amygdala by stimulation of the medial geniculate body. *J Neurosci* 10: 2818–2824, 1990.

Davis M. Neurobiology of fear responses: the role of the amygdala. *J Neuropsychiatry Clin Neurosci* 9: 382–402, 1997.

Davis M, Aggleton JP. The role of the amygdala in conditioned and unconditioned fear and anxiety. In: *The Amygdala*. Oxford, UK: Oxford Univ. Press, 2000, p. 213–287.

Gupta A, Wang Y, Markram H. Organizing principles for a diversity of GABAergic interneurons and synapses in the neocortex. *Science* 287: 273–278, 2000.

Halabisky B, Shen F, Huguenard JR, Prince DA. Electrophysiological classification of somatostatin-positive interneurons in mouse sensorimotor cortex. *J Neurophysiol* 96: 834–845, 2006.

Hammack SE, Mania I, Rainnie DG. Differential expression of intrinsic membrane currents in defined cell types of the anterolateral bed nucleus of the stria terminalis. *J Neurophysiol* 98: 638–656, 2007.

Hutcheon B, Miura RM, Puil E. Subthreshold membrane resonance in neocortical neurons. *J Neurophysiol* 76: 683–697, 1996a.

Hutcheon B, Miura RM, Puil E. Models of subthreshold membrane resonance in neocortical neurons. *J Neurophysiol* 76: 698–714, 1996b.

Izhikevich EM, Desai NS, Walcott EC, Hoppensteadt FC. Bursts as a unit of neural information: selective communication via resonance. *Trends Neurosci* 26: 161–167, 2003.

Josselyn SA, Shi C, Carlezon WA Jr, Neve RL, Nestler EJ, Davis M. Long-term memory is facilitated by cAMP response element-binding protein overexpression in the amygdala. *J Neurosci* 21: 2404–2412, 2001.

Kaneko K, Tamamaki N, Owada H, Kakizaki T, Kume N, Totsuka M, Yamamoto T, Yawo H, Yagi T, Obata K, Yanagawa Y. Noradrenergic excitation of a subpopulation of GABAergic cells in the basolateral amygdala via both activation of nonselective cationic conductance and suppression of resting K(+) conductance: a study using glutamate decarboxylase 67–green fluorescent protein knock-in mice. *Neuroscience* 157: 781–797, 2008.

Katona I, Rancz EA, Acsady L, Ledent C, Mackie K, Hajos N, Freund TF. Distribution of CB1 cannabinoid receptors in the amygdala and their role in the control of GABAergic transmission. *J Neurosci* 21: 9506–9518, 2001.

Kawaguchi Y. Physiological, morphological, and histochemical characterization of three classes of interneurons in rat neostriatum. *J Neurosci* 13: 4908–4923, 1993.

Kawaguchi Y, Kondo S. Parvalbumin, somatostatin and cholecystokinin as chemical markers for specific GABAergic interneuron types in the rat frontal cortex. *J Neurocytol* 31: 277–287, 2002.

Kawaguchi Y, Kubota Y. Neurochemical features and synaptic connections of large physiologically-identified GABAergic cells in the rat frontal cortex. *Neuroscience* 85: 677–701, 1998.

Kennedy JL, Bradwejn J, Koszycki D, King N, Crowe R, Vincent J, Fourie O. Investigation of cholecystokinin system genes in panic disorder. *Mol Psychiatry* 4: 284–285, 1999.

Lawrence JJ, Saraga F, Churchill JF, Statland JM, Travis KE, Skinner FK, McBain CJ. Somatodendritic Kv7/KCNQ/M channels control interspike interval in hippocampal interneurons. *J Neurosci* 26: 12325–12338, 2006.

Liang KC, Hon W, Davis M. Pre- and posttraining infusion of N-methyl-D-aspartate receptor antagonists into the amygdala impair memory in an inhibitory avoidance task. *Behav Neurosci* 108: 241–253, 1994.

Ma Y, Hu H, Berrebi AS, Mathers PH, Agmon A. Distinct subtypes of somatostatin-containing neocortical interneurons revealed in transgenic mice. *J Neurosci* 26: 5069–5082, 2006.

Maren S, Fanselow MS. The amygdala and fear conditioning: has the nut been cracked? *Neuron* 16: 237–240, 1996.

Markram H, Toledo-Rodriguez M, Wang Y, Gupta A, Silberberg G, Wu C. Interneurons of the neocortical inhibitory system. *Nat Rev Neurosci* 5: 793–807, 2004.

Mascagni F, McDonald AJ. Immunohistochemical characterization of cholecystokinin containing neurons in the rat basolateral amygdala. *Brain Res* 976: 171–184, 2003.

Mascagni F, McDonald AJ. A novel subpopulation of 5-HT type 3A receptor subunit immunoreactive interneurons in the rat basolateral amygdala. *Neuroscience* 144: 1015–1024, 2007.

McCormick DA, Connors BW, Lighthall JW, Prince DA. Comparative electrophysiology of pyramidal and sparsely spiny stellate neurons of the neocortex. *J Neurophysiol* 54: 782–806, 1985.

McDonald AJ. Neurons of the bed nucleus of the stria terminalis: a Golgi study in the rat. *Brain Res Bull* 10: 111–120, 1983.

McDonald AJ. Coexistence of somatostatin with neuropeptide Y, but not with cholecystokinin or vasoactive intestinal peptide, in neurons of the rat amygdala. *Brain Res* 500: 37–45, 1989.

McDonald AJ. Projection neurons of the basolateral amygdala: a correlative Golgi and retrograde tract tracing study. *Brain Res Bull* 28: 179–185, 1992.

McDonald AJ. Glutamate and aspartate immunoreactive neurons of the rat basolateral amygdala: colocalization of excitatory amino acids and projections to the limbic circuit. *J Comp Neurol* 365: 367–379, 1996.

McDonald AJ, Betette RL. Parvalbumin-containing neurons in the rat basolateral amygdala: morphology and co-localization of calbindin-D(28k). *Neuroscience* 102: 413–425, 2001.

McDonald AJ, Mascagni F. Colocalization of calcium-binding proteins and GABA in neurons of the rat basolateral amygdala. *Neuroscience* 105: 681–693, 2001a.

McDonald AJ, Mascagni F. Localization of the CB1 type cannabinoid receptor in the rat basolateral amygdala: high concentrations in a subpopulation of cholecystokinin-containing interneurons. *Neuroscience* 107: 641–652, 2001b.

McDonald AJ, Mascagni F. Immunohistochemical characterization of somatostatin containing interneurons in the rat basolateral amygdala. *Brain Res* 943: 237–244, 2002.

McDonald AJ, Mascagni F. Differential expression of Kv3.1b and Kv3.2 potassium channel subunits in interneurons of the basolateral amygdala. *Neuroscience* 138: 537–547, 2006.

McDonald AJ, Pearson JC. Coexistence of GABA and peptide immunoreactivity in non-pyramidal neurons of the basolateral amygdala. *Neurosci Lett* 100: 53–58, 1989.

Meyer AH, Katona I, Blatow M, Rozov A, Monyer H. In vivo labeling of parvalbumin-positive interneurons and analysis of electrical coupling in identified neurons. *J Neurosci* 22: 7055–7064, 2002.

Morales M, Bloom FE. The 5-HT3 receptor is present in different subpopulations of GABAergic neurons in the rat telencephalon. *J Neurosci* 17: 3157–3167, 1997.

Muller J, Corodimas KP, Fridel Z, LeDoux JE. Functional inactivation of the lateral and basal nuclei of the amygdala by muscimol infusion prevents fear conditioning to an explicit conditioned stimulus and to contextual stimuli. *Behav Neurosci* 111: 683–691, 1997.

Muller JF, Mascagni F, McDonald AJ. Synaptic connections of distinct interneuronal subpopulations in the rat basolateral amygdalar nucleus. *J Comp Neurol* 456: 217–236, 2003.

Muller JF, Mascagni F, McDonald AJ. Coupled networks of parvalbumin-immunoreactive interneurons in the rat basolateral amygdala. *J Neurosci* 25: 7366–7376, 2005.

Muller JF, Mascagni F, McDonald AJ. Postsynaptic targets of somatostatin-containing interneurons in the rat basolateral amygdala. *J Comp Neurol* 500: 513–529, 2007.

Naldini L, Blomer U, Gallay P, Ory D, Mulligan R, Gage FH, Verma IM, Trono D. In vivo gene delivery and stable transduction of nondividing cells by a lentiviral vector. *Science* 272: 263–267, 1996.

Pape H-C, Driesang RB. Ionic mechanisms of intrinsic oscillations in neurons of the basolateral amygdaloid complex. *J Neurophysiol* 79: 217–226, 1998.

Pawelzik H, Hughes DI, Thomson AM. Physiological and morphological diversity of immunocytochemically defined parvalbumin- and cholecystokinin-positive interneurones in CA1 of the adult rat hippocampus. *J Comp Neurol* 443: 346–367, 2002.

Paxinos G, Watson C. *The Rat Brain in Stereotaxic Coordinates.* San Diego, CA: Elsevier Academic, 2005.

Pike FG, Goddard RS, Suckling JM, Ganter P, Kasthuri N, Paulsen O. Distinct frequency preferences of different types of rat hippocampal neurones in response to oscillatory input currents. *J Physiol* 529: 205–213, 2000.

Protopopescu X, Pan H, Tuescher O, Cloitre M, Goldstein M, Engelien W, Epstein J, Yang Y, Gorman J, LeDoux J, Silbersweig D, Stern E. Differential time courses and specificity of amygdala activity in posttraumatic stress disorder subjects and normal control subjects. *Biol Psychiatry* 57: 464–473, 2005.

Rainnie DG. Serotonergic modulation of neurotransmission in the rat basolateral amygdala. *J Neurophysiol* 82: 69–85, 1999.

Rainnie DG, Mania I, Mascagni F, McDonald AJ. Physiological and morphological characterization of parvalbumin-containing interneurons of the rat basolateral amygdala. *J Comp Neurol* 498: 142–161, 2006.

Rauch SL, Whalen PJ, Shin LM, McInerney SC, Macklin ML, Lasko NB, Orr SP, Pitman RK. Exaggerated amygdala response to masked facial stimuli in posttraumatic stress disorder: a functional MRI study. *Biol Psychiatry* 47: 769–776, 2000.

Ressler KJ, Paschall G, Zhou XL, Davis M. Regulation of synaptic plasticity genes during consolidation of fear conditioning. *J Neurosci* 22: 7892–7902, 2002.

Rudy B, McBain CJ. Kv3 channels: voltage-gated K^+ channels designed for high-frequency repetitive firing. *Trends Neurosci* 24: 517–526, 2001.

Sananes CB, Davis M. N-Methyl-D-aspartate lesions of the lateral and basolateral nuclei of the amygdala block fear-potentiated startle and shock sensitization of startle. *Behav Neurosci* 106: 72–80, 1992.

Schwindt PC, Spain WJ, Foehring RC, Stafstrom CE, Chubb MC, Crill WE. Multiple potassium conductances and their functions in neurons from cat sensorimotor cortex in vitro. *J Neurophysiol* 59: 424–449, 1988.

Smith Y, Paré J-F, Paré D. Differential innervation of parvalbumin-immunoreactive interneurons of the basolateral amygdaloid complex by cortical and intrinsic inputs. *J Comp Neurol* 416: 496–508, 2000.

Somogyi P, Klausberger T. Defined types of cortical interneurone structure space and spike timing in the hippocampus. *J Physiol Online* 562: 9–26, 2005.

Sosulina L, Meis S, Seifert G, Steinhauser C, Pape HC. Classification of projection neurons and interneurons in the rat lateral amygdala based upon cluster analysis. *Mol Cell Neurosci* 33: 57–67, 2006.

Sugino K, Hempel CM, Miller MN, Hattox AM, Shapiro P, Wu C, Huang ZJ, Nelson SB. Molecular taxonomy of major neuronal classes in the adult mouse forebrain. *Nat Neurosci* 9: 99–107, 2006.

Sun N, Cassell MD. Intrinsic GABAergic neurons in the rat central extended amygdala. *J Comp Neurol* 330: 381–404, 1993.

Szinyei C, Heinbockel T, Montagne J, Pape HC. Putative cortical and thalamic inputs elicit convergent excitation in a population of GABAergic interneurons of the lateral amygdala. *J Neurosci* 20: 8909–8915, 2000.

Szinyei C, Narayanan RT, Pape HC. Plasticity of inhibitory synaptic network interactions in the lateral amygdala upon fear conditioning in mice. *Eur J Neurosci* 25: 1205–1211, 2007.

Szinyei C, Stork O, Pape HC. Contribution of NR2B subunits to synaptic transmission in amygdaloid interneurons. *J Neurosci* 23: 2549–2556, 2003.

Tiscornia G, Singer O, Verma IM. Production and purification of lentiviral vectors. *Nat Protoc* 1: 241–245, 2006.

Ward JH Jr. Hierarchical grouping to optimize an objective function. *J Am Stat Assoc* 58: 236–244, 1963.

Woodruff AR, Sah P. Inhibition and synchronization of basal amygdala principal neuron spiking by parvalbumin-positive interneurons. *J Neurophysiol* 98: 2956–2961, 2007a.

Woodruff AR, Sah P. Networks of parvalbumin-positive interneurons in the basolateral amygdala. *J Neurosci* 27: 553–563, 2007b.